# EXPERIMENTAL APPLICATION OF $\ell_1$-OPTIMAL CONTROL IN ATOMIC FORCE MICROSCOPY

**Jochen M. Rieber** [*], **Georg Schitter** [**], **Andreas Stemmer** [**], **Frank Allgöwer** [*,1]

[*] *Institute for Systems Theory in Engineering, University of Stuttgart, Pfaffenwaldring 9, 70550 Stuttgart, Germany*
[**] *Nanotechnology Group, Swiss Federal Institue of Technology, ETH Zentrum CLA, 8092 Zürich, Switzerland*

Abstract: This paper presents an experimental application of $\ell_1$-optimal control. In an atomic force microscope, the vertical position of the piezoelectric tube scanner and thus the cantilever deflection is controlled using a 2-degree-of-freedom control design. The last recorded scan line is fed forward whereas a feedback controller provides stability and setpoint control. Experimental results verify the performance of the approach and give insight into applicability, design, and implementation aspects of $\ell_1$-optimal controllers. 

Keywords: $\ell_1$-optimal control, 2-DOF control design, atomic force microscopy, experimental application.

## 1. INTRODUCTION

In the area of linear optimal and robust control, powerful methods for disturbance rejection have been established during the last 15 years. One important framework is $\ell_1$-optimal control, treated comprehensively in (Dahleh and Diaz-Bobillo, 1995; Dahleh and Khammash, 1993) and references therein. The $\ell_1$ control problem addresses persistent bounded disturbances, as well as direct time-domain performance specifications like overshoot, bounded magnitude, bounded slope, or actuator saturation. Recent advances include a novel controller synthesis method (Khammash, 2000), the solution to the robust performance problem in face of structured uncertainties (Khammash et al., 2001), as well as extensions to mixed performance synthesis (Sznaier and Bu, 1998) and gain-scheduling (Rieber and Allgöwer, 2003), for example. Despite fruitful theoretical developments, real-world applications of $\ell_1$-optimal control are quite rare so far, see (Malaterre and Khammash, 2000; Tadeo et al., 1998; Tadeo and Grimble, 2002).

In this paper, the synthesis of $\ell_1$ controllers for an atomic force microscope (AFM) is presented and the resulting controllers are experimentally tested. AFMs are used to trace the topography of a nanoscale specimen by a sharp tip supported on a micro-mechanical cantilever (Binnig et al., 1986). Fig. 1 graphically depicts a standard feedback-controlled AFM system. The spatially resolved topography is measured while scanning the sample laterally under the probing tip. To this end, the cantilever deflection due to the sample's topography is monitored by an optical lever and a segmented photo diode. During this process, the sample is moved laterally and vertically by means of a piezoelectric tube scanner. Detailed descriptions of AFM components and of the AFM function are given in (Binnig et al., 1986; Sarid, 1994). Control applications for AFMs are reported in (Schitter et al., 2004; Salapaka and Sebastian, 2003), for example.

[1] Corresponding author: F. Allgöwer.
Email: allgower@ist.uni-stuttgart.de

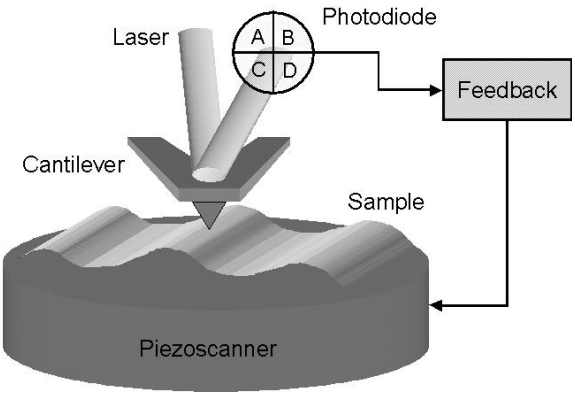


Fig. 1. Graphical scheme of an AFM setup.

Commercial AFM controllers usually apply a proportional-integral (PI) element to control the cantilever deflection. High resolution images of the specimen topography are typically obtained at relatively low speeds. Fast imaging usually results in image distortions due to cantilever deflections and piezo tube oscillations. In contrast, here the $\ell_1$ approach is applied to vertical position control of an AFM for several reasons. First, the mentioned disadvantages of standard PI-controlled AFM systems should be alleviated. Second, applications of $\ell_1$ theory to fast mechanical systems are not available to the best of the authors' knowledge. Third, it is believed that $\ell_1$ control is particularly well-suited for this kind of problem, since the task at hand is to provide a low cantilever deflection amplitude during the scanning process and minimal overshoot. A 2-degree-of-freedom (2-DOF) control system design is proposed for control of the piezo scanner vertical position, similar to ideas expressed in (Schitter et al., 2004). The controller design is based on a 5th-order identified model of the piezo scanner, exhibiting non-minimum phase behavior (Schitter et al., 2004). An $\ell_1$ feedback controller guarantees closed-loop stability, disturbance rejection and asymptotical setpoint control. In addition, an $\ell_1$ feedforward filter takes advantage from the fact that two adjacent scan lines normally are quite similar, and tracks the tube scanner to the last recorded scan line, delayed by one period of the scanning motion. Experimental results demonstrate the performance of the $\ell_1$-controlled AFM system.

Such an application with important frequency domain characteristics, oscillatory behavior and nanometer accuracy is chosen in order to pose a challenge to $\ell_1$ control. Thus the goal of this paper is not only the control of such an AFM system per se, but more importantly to apply the $\ell_1$ method to a challenging real-world problem. This helps in gaining insight into design and applicability of $\ell_1$ controllers. Specifically, some reasonable design procedures, weight selection, and implementation aspects are discussed.

## 2. ATOMIC FORCE MICROSCOPY

The AFM under consideration is a Nanoscope-IIIa MultiMode-AFM (Veeco, Santa Barbara, USA). All real-time operations are run on a digital signal processor (DSP) DS1005 with 16-bit A/D and D/A converters (dSpace, Paderborn, Germany).

### *2.1 AFM Operation*

As described in the introduction, an AFM is operated by moving the piezo scanner together with the sample laterally and vertically under the cantilever tip. In contact mode, the tip permanently touches the specimen. In the so-called "constant force mode", the cantilever deflection and thus the tip-sample interaction force is held constant in a closed-loop operation. The feedback loop compensates changes in the deflection signal of the cantilever (due to the sample's topography) by varying the position of the sample along the vertical ($z$) direction. Thus the sample topography may be seen as a "disturbance" to the AFM system. The actual topography information then corresponds to the voltage applied to the scanner in $z$-direction (Schitter et al., 2004). Spatially resolved images of the sample surface are drawn by recording the feedback-generated voltage applied to the $z$-axis of the scanner piezo simultaneously with the lateral position of the sample. A setpoint in the control-loop predetermines the nominal value of the tip-sample interaction force.

### *2.2 AFM Modeling*

Physical modeling of the AFM dynamics and tip-sample interaction is a main topic in (Schitter et al., 2001; Stark et al., 2004). The tip-sample interaction can be regarded as a static feedback that affects the cantilever dynamics (Stark et al., 2004). In contact mode, the first resonance frequency of the cantilever that is supported by the sample is much higher than the control bandwidth, and the cantilever dynamics thus do not have to be taken into account in the control problem. Therefore, only the dynamics of the piezo scanner are considered from hereon, whereas the photo diode and cantilever dynamics result in a constant gain. Moreover, this paper focuses on control of the tube scanner's vertical position only. Thus all lateral dynamics are not explicitly modeled or taken into account during controller design. However, a compensation in scanning direction is applied to avoid lateral oscillations of the tube scanner during the scanning motion. This compensation is an open-loop model-based controller as derived in (Schitter and Stemmer, 2004).

Instead of modeling the piezo scanner based on first principles, a sub-space identification is ap-

plied in (Schitter et al., 2001; Schitter et al., 2004), resulting in the mathematical model

$$G(z)=\frac{0.0102z^4+0.269z^3+2.76z^2-1.25z+2.49}{z^5-2.35z^4+2.83z^3-1.85z^2+0.701z-0.178} \quad (1)$$

of the vertical dynamics, with a sampling time of 16.5 $\mu$s. Gains of the voltage amplifier and of the photo diode are included. This model exhibits a fundamental resonance at a frequency of about 8.5 kHz as well as an anti-resonance at about 12 kHz. Comparisons between simulated and experimental data validated the identified model (Schitter et al., 2004).

## 3. CONTROLLER DESIGN

### *3.1 Introduction to $\ell_1$-Optimal Control*

In $\ell_1$-optimal control, discrete-time linear time-invariant (LTI) multi-input/multi-output (MIMO) systems $P$ with state-space description

$$\begin{bmatrix} x(k+1) \\ z(k) \\ y(k) \end{bmatrix} = \begin{bmatrix} A & B_1 & B_2 \\ C_1 & D_{11} & D_{12} \\ C_2 & D_{21} & D_{22} \end{bmatrix} \begin{bmatrix} x(k) \\ w(k) \\ u(k) \end{bmatrix} \quad (2)$$

are considered, where the variables denote states $x \in \mathbb{R}^n$, reference signals and exogenous disturbances $w \in \mathbb{R}^{q_1}$, control inputs $u \in \mathbb{R}^{q_2}$, performance outputs $z \in \mathbb{R}^{p_1}$ and measurements $y \in \mathbb{R}^{p_2}$. Such a description may include static and dynamic weighting factors. Assumptions on the plant are stabilizability of $(A, B_2)$ and detectability of $(A, C_2)$.

The exogenous disturbances are allowed to be elements of $\ell_\infty^n$, which is the space of vector-valued right-sided bounded real sequences $s = \{s(k)\}_{k=0}^\infty$ with $s(k) = [s_1(k), \ldots, s_n(k)]^T$ and the norm $\|s\|_\infty := \max_{1\le i\le n} \sup_k |s_i(k)|$. This means that the signals in this space are of finite amplitude, but not necessarily of finite energy. Recall that the $\mathcal{Z}$-transform of a one-sided sequence $s$ is defined as $S(z) := \sum_{k=0}^\infty s(k) z^{-k}$.

To have a measure of worst-case signal amplification, the $\ell_\infty$-gain between input $w$ and output $z$ of a system is introduced, which is the $\ell_\infty$-induced norm of the system operator $T : \ell_\infty^n \to \ell_\infty^m$, defined by

$$\|T\|_{\infty-\text{ind}} := \sup_{w\in\ell_\infty, w\neq 0} \frac{\|Tw\|_\infty}{\|w\|_\infty} .$$

For an LTI operator or transfer function, the $\ell_\infty$-induced norm is the $\ell_1$-norm of its impulse response matrix. To this end, note that the vector space $\ell_1^{m\times n}$ is the space of matrix-valued right-sided absolutely summable real sequences, equipped with the norm

$$\|s\|_1 := \max_{1\le i\le m} \sum_{j=1}^n \sum_{k=0}^\infty |s_{ij}(k)|.$$

The goal of standard $\ell_1$-optimal control is to design an LTI output-feedback controller $u = Ky$ that internally stabilizes the closed loop and minimizes its $\ell_\infty$-gain. Mathematically speaking, $K$ is the argument of the optimization

$$\gamma^* := \inf_K \|T(P,K)\|_1 , \quad (3)$$

where the closed loop is represented by the $p_1 \times q_1$ impulse response matrix $T(P, K)$.

The usefulness of the $\ell_1$ approach lies in the support of intuitive performance specifications directly in the time-domain. It is possible to capture requirements like bounded control error, actuator saturation, bounded slope, no overshoot etc., all in the presence of non-vanishing disturbances like step signals. An in-depth treatment of the fundamentals on $\ell_1$ control and of its motivation is found in (Dahleh and Diaz-Bobillo, 1995; Dahleh and Khammash, 1993).

### *3.2 Synthesis of $\ell_1$-Suboptimal Controllers*

Another feature of $\ell_1$-optimal control is the possibility to synthesize (sub)optimal controllers by means of linear programs, which makes the method computationally very attractive. For general MIMO systems, several approaches to compute an $\ell_1$-(sub)optimal controller exist. Two of them, namely the Finitely-Many-Variables/Finitely-Many-Equations method and the Delay Augmentation method, are derived from the characterization of optimal solutions with interpolation conditions (Dahleh and Diaz-Bobillo, 1995). A third approach, the Scaled-$Q$ method (SQM), has been introduced recently (Khammash, 2000). Other methods rely on $\mathcal{H}_2$ approximations or polynomial approaches. The SQM is applied in this paper because of certain advantages. First, no assumptions on plant transfer zeros and ordering of outputs are needed. Second, numerical delicacies in obtaining the optimal controller are minimal. Third, SQM possesses converging lower and upper bounds of the optimal solution. As is general for $\ell_1$-optimal controllers, their resulting order may be high, and a large number of (in-)equalities may be involved in their computation.

A procedure for synthesizing a suboptimal controller according to the SQM consists of several steps. From the generalized plant (2), a Youla parameterization of all stable closed-loop transfer functions $T(z)$ is calculated as

$$T(z) = H(z) - V_1(z)Q(z)V_2(z) ,$$

where $H$, $V_1$ and $V_2$ can be obtained from the plant description (2) via state-space formulas, see (Zhou et al., 1996; Dahleh and Diaz-Bobillo, 1995). The free parameter $Q(z)$, whose impulse response $Q$ has to be an element of $\ell_1$, is chosen such that $\|T\|_1$ becomes minimal. The general $\ell_1$ optimization (3) may be transformed into finite-dimensional linear programs for monotonically

converging lower and upper bounds of $\gamma^*$. From the solution of the upper bound minimization, the Youla parameter $Q$ and therefore the controller $K$ is recovered, see (Zhou et al., 1996; Dahleh and Diaz-Bobillo, 1995). A detailed description of the derivation and of the properties of the SQM is given in (Khammash, 2000).

### *3.3 Controller Design for the AFM*

The task under consideration is controlling the AFM cantilever deflection by varying the position of the sample along the $z$-direction. The voltage applied to the piezo tube is seen as control input, whereas the photo diode signal is the measurement provided to the controller. The setpoint predetermines the desired contact force between tip and sample. As already mentioned in Section 2.2, the vertical dynamics play the major role during controller design.

The controller design in this contribution consists of two steps. Ideas similar to the ones described in (Schitter et al., 2004) are taken up and adapted to the $\ell_1$ framework and to the task at hand. First, an $\ell_1$ feedback controller is designed, guaranteeing closed-loop stability, asymptotical setpoint control and disturbance rejection. A block diagram of the control loop is shown in Fig. 2(a), from which the generalized plant is derived. The "Scanner" block represents the model $G$, which is precompensated by

$$\bar{K}_c(z) = \underbrace{\frac{e_2 z^2 + e_1 z + e_0}{f_2 z^2 + f_1 z + f_0}}_{K_c(z)} \cdot \underbrace{\frac{1}{z-1}}_{K_{int}(z)} \,. \qquad (4)$$

Its first part $K_c$ deals with the resonance of the plant, and the coefficients $e_i$ and $f_i$ are chosen such that the stable plant resonance is approximately canceled and $K_c$ is stable. This compensation improves the result of the subsequent $\ell_1$ design step. The integrator $K_{int}$ provides zero steady-state error for step disturbances. The "Feedback" block represents the $\ell_1$ controller to be designed. The exogenous input $r_{FB}$ can be interpreted as the setpoint and the sample topography "disturbance". The generalized plant (2) with inputs $[w, u]^T = [r_{FB}, u]^T$ and outputs $[z^T, y]^T = [z_{FB1}, z_{FB2}, y]^T$ is obtained from Fig. 2(a) (after removing the feedback block to be designed) as the state-space description of

$$P(z) = \begin{bmatrix} W_{e1}(z) & 0 & 0 \\ 0 & W_{u1}(z) & 0 \\ 0 & 0 & 1 \end{bmatrix} \begin{bmatrix} 1 & -G(z)\bar{K}_c(z) \\ 0 & 1 \\ 1 & -G(z)\bar{K}_c(z) \end{bmatrix}.$$

Since the minimization in $\ell_1$-optimal control takes place in the time-domain, the weight selection has to follow different criteria than for example the frequency domain based approach of $\mathcal{H}_\infty$ methods. In this application, the weight $W_{e1}$ is

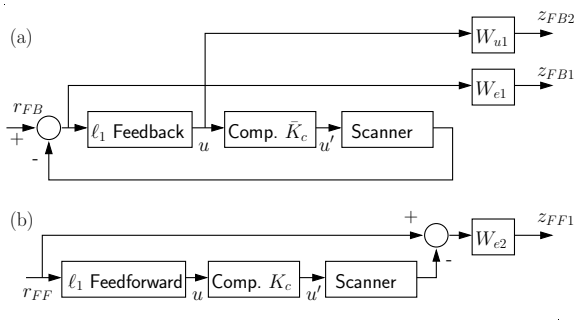


Fig. 2. Control setup of the feedback part (a) and the feedforward part (b).

set to a constant penalizing the control error. First- or second-order dynamic weights did not improve the results while increasing the controller-order, which may be prohibitive for real-time implementation. In the same way, $W_{u1}$ is chosen to be a constant penalizing the control action $u$ and influencing the actuator signal amplitude and the bandwidth of the closed loop. The theoretically optimal performance of $\gamma^\star = 2$ is approximated with an error in the order of $10^{-3}$ (that is with the upper bound $\bar{\gamma} = 2.00$) by a controller of order 31. A suboptimal controller of order 16 achieves $\bar{\gamma} = 2.32$. Both controllers possess a sparse dynamic matrix, which alleviates implementation problems arising from their high order.

In a second step, a pure open-loop feedforward controller is designed according to the setup in Fig. 2(b). The "Scanner" block is precompensated by the transfer function $K_c(z)$, see (4). The "Feedforward" block stands for the $\ell_1$ filter to be designed. Now the exogenous input $r_{FF}$ is interpreted as a topography signal to be tracked. A description corresponding to Fig. 2(b) is

$$P(z) = W_{e2}(z)(1 - G(z)K_c(z)Q(z)) \,,$$

where $Q(z)$ represents the feedforward filter. With help of the weight $W_{e2}$, the error between this reference and the scanner output is penalized. Here $W_{e2} = 1$. For design of the feedforward filter, additional time-domain conditions are imposed. In particular, a low-overshoot restriction $z_{FF1} \geq -2 \cdot 10^{-4}$ in response to a unit step input prevents too aggressive tracking. Additionally, an exponential decay of the error in response to a unit step input is demanded via $z_{FF1}(k) \leq a^{k-3}$ for $0 < a < 1$, $k \geq 3$. The resulting 4th-order filter achieves $\bar{\gamma} = 2.00$.

The feedback and feedforward controllers are combined as shown in the block diagram of the implemented controller in Fig. 3. The feedback path uses the error between the photo diode output and the setpoint to keep the cantilever deflection constant. The sample topographical information is calculated by feeding the voltage signal into the "Scanner Simulation" block, that is a model of the piezo scanner. The simulated topography of

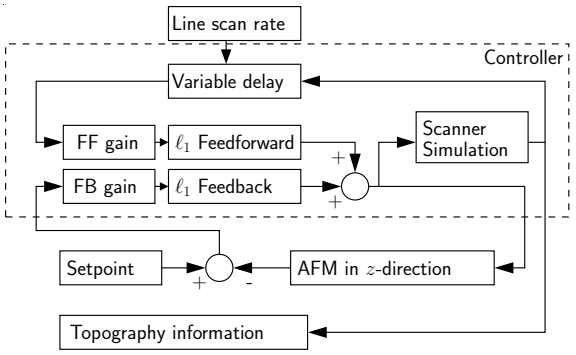


Fig. 3. Block diagram of the implemented controller in closed loop with the AFM.

the last recorded scan line, delayed by one period of the lateral scanning motion, is then tracked by the feedforward filter. The two blocks "FF gain" (feedforward gain) and "FB gain" (feedback gain) are variable gains used for online fine-tuning and for investigating the contributions of feedforward and feedback in the control input signal (Schitter et al., 2004).

To summarize, an $\ell_1$ control setup with constant weights is investigated. Controller tuning is very easy since the weights and performance specifications have a direct and intuitive meaning – namely penalizing the maximum amplitudes of the control error or of the actuator signal, respectively. Furthermore, additional conditions on the overshoot and on error decay are incorporated in a direct quantitative way. In contrast, both PI controller tuning and frequency weight selection in the $\mathcal{H}_\infty$ framework require a considerably higher amount of experience and system theoretical insight. The whole $\ell_1$ controller design process is easily performed using standard software for linear programming like MATLAB. Finally, the SQM allows for design of suboptimal controllers of any given order which facilitates implementation even on slow DSP systems while sacrificing some performance as seen on the resulting values of $\bar{\gamma}$.

## 4. EXPERIMENTAL RESULTS

For the following experiments, a calibration grid with near vertical edge drop-off of 200 nm is scanned at different speeds. The controllers' performances are compared mainly based on the amplitude of the cantilever deflection signal. In all cases, the above-mentioned compensation of the lateral scanning motion is active (Schitter and Stemmer, 2004).

The experiments compare a well-tuned PI feedback controller to the proposed $\ell_1$ control structure including the feedforward and feedback parts. In Fig. 4, the recorded images of the calibration grid and the corresponding deflection signals are shown for both $\ell_1$ 2-DOF-control and PI feedback

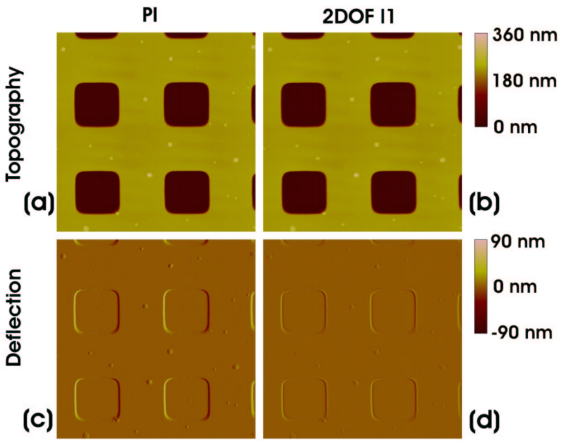


Fig. 4. Comparison of 2D-images obtained with PI- and $\ell_1$-2-DOF-controlled AFM at 10 Hz scan rate. Scan direction is from right to left. The dimensions of the displayed sections are 25 $\mu$m by 25 $\mu$m each. Bright and dark spots in (c) and (d) (differing from the predominating color) indicate a large control error.
(a) Topographical data, PI controller,
(b) Topographical data, $\ell_1$ controller,
(c) Cantilever deflection, PI controller,
(d) Cantilever deflection, $\ell_1$ controller.

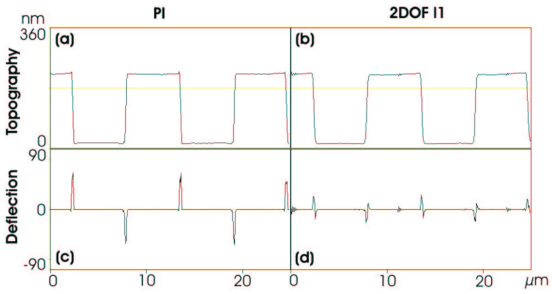


Fig. 5. Comparison of cross section cuts obtained with PI- and $\ell_1$-controlled AFM at 10 Hz scan rate. Sections (a)–(d) are as in Fig. 4.

at a scanning rate of 10 lines per second, that is 10 Hz. Corresponding cross section cuts in Fig. 5 display the obtained topography information and the cantilever deflection at one specific scan line. It is clear from Figs. 5(c) and (d) that the cantilever deflection exhibits considerably higher values in the PI-controlled case. This means that higher force variations occur during the scanning process, leading to measurement errors in the topographical data and possibly to damages of the tip and/or the sample. The $\ell_1$ controller clearly reduces these undesirable effects.

To increase efficiency in nano imaging, application of high scanning rates are very desirable while keeping imaging accuracy. This is usually not attainable with standard PI controllers. Thus, a second set of experiments conducted at a scanning rate of 30 Hz is performed with a re-tuned PI controller and the same $\ell_1$ controller as before.

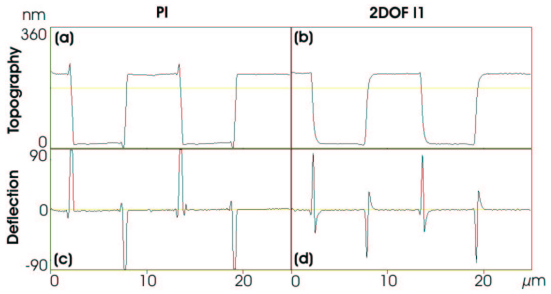


Fig. 6. Comparison of cross section cuts obtained with PI- and $\ell_1$-controlled AFM at 30 Hz scan rate. Sections (a)–(d) are as in Fig. 4.

The results are shown in Fig. 6. Comparing Fig. 6 with Fig. 5, the PI-related curves exhibit a heavy degradation with respect to cantilever deflection and overshoot in the measured topography. The cantilever deflection even saturates. In contrast, the $\ell_1$ controller still provides a relatively smooth, low-overshoot transition at the detected edges, although the cantilever deflection is also higher than for 10 Hz scan rate. Further experiments showed that in the case where the $\ell_1$ feedforward filter is switched off, still a smooth tracking of the topography with almost no overshoot occurs, whereas with PI feedback a significant overshoot is visible.

This application proves the suitability of $\ell_1$-optimal controllers for challenging real-world problems. The time-domain based method can even cope with a system exhibiting strong frequency domain characteristics, oscillatory and non-minimum phase behavior. The experimental results moreover demonstrate the superior performance of the $\ell_1$-controlled system compared to a well-tuned PI controller commonly used in commercial AFM products. Finally, the ease of design and intuitiveness of performance specifications is clearly visible. One disadvantage of $\ell_1$ control, namely the generally high controller order, is circumvented by applying slightly suboptimal low-order controllers. A direct trade-off between controller order and achieved performance facilitates the application and allows for good results in the suboptimal case. Further performance enhancement is to be expected from a higher-order optimal controller. The necessary computation power is available in newer AFM generations which are more and more equipped with field-programmable gate arrays (FPGAs).

## 5. CONCLUSIONS

This contribution presents a 2-degree-of-freedom controller design for an atomic force microscope in the $\ell_1$-optimality framework. The vertical position of the piezoelectric tube scanner is stabilized with help of a feedback controller, whereas a feedforward filter tracks the topography in a high-performance manner. The study in this paper gives insight into the applicability of $\ell_1$ controllers, appropriate control structures, and performance specifications. Moreover, discussions of implementation aspects point to a trade-off between controller performance and controller order. Finally, the experimental results prove the applicability of $\ell_1$-(sub)optimal controllers for challenging real-world problems, and validate their superior performance for the AFM system compared to a well-tuned PI controller used in commercial products.

## REFERENCES


Binnig, G., C.F. Quate and C. Gerber (1986). Atomic force microscope. *Physical Review Letters*, **56**(9), 930–933.

Dahleh, M.A. and I.J. Diaz-Bobillo (1995). *Control of uncertain systems: a linear programming approach.* Prentice-Hall, Upper Saddle River, NJ, USA.

Dahleh, M.A. and M.H. Khammash (1993). Controller design for plants with structured uncertainty. *Automatica*, **29**, 37–56.

Khammash, M. (2000). A new approach to the solution of the $\ell_1$ control problem: The scaled-$Q$ method. *IEEE Trans. Automatic Control*, **45**, 180–187.

Khammash, M., M.V. Salapaka and T. Van Voorhis (2001). Robust synthesis in $\ell_1$: a globally optimal solution. *IEEE Trans. Automatic Control*, **46**, 1744–1754.

Malaterre, P.O. and M. Khammash (2000). $\ell_1$ controller design for a high-order 5-pool irrigation canal system. *Proc. 39th IEEE Conf. Decision and Control*, Sydney, Australia, pp. 3188–3193.

Rieber, J.M. and F. Allgöwer (2003). An approach to gain-scheduled $\ell_1$-optimal control of linear parameter-varying systems. *Proc. 42nd IEEE Conf. Decision and Control*, Maui, HI, USA, pp. 6109–6114.

Sarid, D. (1994). *Scanning Force Microscopy.* Oxford University Press, New York, NY, USA.

Schitter, G., P. Menold, H.F. Knapp, F. Allgöwer and A. Stemmer (2001). High performance feedback for fast scanning atomic force microscopes. *Review Scientific Instruments*, **72**(8), 3320–3327.

Schitter, G., F. Allgöwer and A. Stemmer (2004). A new control strategy for high-speed atomic force microscopy. *Nanotechnology*, **15**, 108–114.

Schitter, G. and A. Stemmer (2004). Identification and open-loop tracing control of a piezoelectric tube scanner for high-speed scanning-probe microscopy. *IEEE Trans. Control Systems Technology*, **12**(3), 449–454.

Salapaka, S. and A. Sebastian (2003). Control of nanopositioning devices. *Proc. 42nd IEEE Conf. Decision and Control*, Maui, HI, USA, pp. 2644–2649.

Stark, R.W., G. Schitter, M. Stark, R. Guckenberger, and A. Stemmer (2004). State-space model of freely vibrating and surface-coupled cantilever dynamics in atomic force microscopy. *Physical Review B*, **69**, 085412-1–085412-9.

Sznaier, M. and J. Bu (1998). Mixed $l_1/\mathcal{H}_\infty$ control of MIMO systems via convex optimization. *IEEE Trans. Automatic Control*, **43**, 1229–1241.

Tadeo, F., A. Holohan and P. Vega (1998). $\ell_1$-optimal control of a pH plant. *Computers and Chemical Engineering*, **22**, S459–S466.

Tadeo, F. and M.J. Grimble (2002). Advanced control of a hydrogen reformer. *IEE Computing and Control Eng. Journal*, **13**, 305–314.

Zhou, K., J.C. Doyle and K. Glover (1996). *Robust and Optimal Control.* Prentice-Hall, Upper Saddle River, NJ, USA.